Canadian Mineralogist
Vol. 28, pp. 835-854 (1990)

APATITE OF THE DUFEK INTRUSION: DISTRIBUTION, PARAGENESIS, AND CHEMISTRY

JAMES L. DRINKWATER, GERALD K. CZAMANSKE AND ARTHUR B. FORD
U.S. Geological Survey, 345 Middlefield Road, Menlo Park, California 94025, U.S.A.

ABSTRACT

Apatite in the Dufek intrusion of Antarctica is F-rich and exhibits systematic variations in contents of Cl, F, Fe, Sr, and rare-earth elements (*REE*s). Four types of apatite are distinguished on the basis of morphology, grain size, and textural relations: 1) cumulus, 2) early postcumulus (euhedral forms), 3) late postcumulus (anhedral forms), and 4) noncumulus primocryst. Cumulus apatite is relatively rich in F, Fe, and Sr, and poor in Cl and *LREE*s, whereas postcumulus apatite commonly contains more Cl and *LREE*s, and less F than cumulus apatite. Apatite primocrysts of the capping granophyre are depleted in Cl and enriched in *REE*s. Cl, F, Fe, and *REE*s are partitioned between the two types of postcumulus apatite, with euhedral, early-postcumulus grains typically containing less F, more Cl and Fe, and having higher Ce/Y ratios than anhedral, late-postcumulus grains. Large subhedral apatite sporadically occurs in anorthosite and leucogabbro below the main cumulus-apatite horizon, and shows textural and chemical evidence of being recycled cumulus apatite, deposited by current activity. Whole-rock P contents follow patterns generally comparable to those described for other layered mafic intrusions, but are unusually high in cumulates of the Forrestal Range section. Iron-rich biotite occurs in thin (5–15 μm) infilled cavities parallel to the *c* axes of some well-formed cumulus and early-postcumulus apatite crystals.

Keywords: apatite, Dufek intrusion, phosphorus, rare-earth elements, Antarctica.

SOMMAIRE

L'apatite du complexe intrusif de Dufek, dans l'Antarctique, est riche en fluor et fait preuve de variations systématiques en teneurs de Cl, F, Fe, Sr et des terres rares. Nous distinguons quatre types d'apatite selon la morphologie, la granulométrie, et les relations texturales: 1) apatite cumulative, 2) apatite post-cumulative précoce (formes idiomorphes), 3) apatite post-cumulative tardive (formes xénomorphes), et 4) cristaux primaires d'origine non cumulative. L'apatite cumulative est relativement enrichie en F, Fe, et Sr, et appauvrie en Cl et les terres rares légères, tandis que l'apatite post-cumulative contient couramment de plus fortes concentrations de Cl et des terres rares légères, et moins de F, que l'apatite cumulative. Les cristaux primaires de la couche de granophyre sont appauvris en Cl et enrichis en terres rares. Cl, F, Fe et les terres rares sont répartis entre les deux types d'apatite post-cumulative: l'apatite précoce idiomorphe contient typiquement moins de F, plus de Cl et de Fe, et possède un rapport Ce/Y plus élevé que les grains tardifs xénomorphes. L'apatite à gros grains subidiomorphes qui se trouvent dans les niveaux d'anorthosite et de leucogabbro en dessous de l'horizon principal à cumulats d'apatite auraient, selon l'évidence texturale et chimique, une origine par recyclage de l'apatite cumulative, avec déposition par courants magmatiques. Les teneurs en P des roches globales sont généralement comparables à celles d'autres complexes stratiformes mafiques, quoiqu'elles sont anormalement élevées dans la section de Forrestal Range. Une biotite ferrifère occupe la cavité remplie (5-15 μm) parallèle à l'axe *c* de certains cristaux idiomorphes d'apatite cumulative et post-cumulative précoce.

(Traduit par la Rédaction)

Mots-clés: apatite, complexe intrusif de Dufek, phosphore, terres rares, Antarctique.

INTRODUCTION

The Dufek intrusion is a huge layered mafic body of Jurassic age located in the northern Pensacola Mountains of Antarctica (Fig. 1; Ford 1970). The intrusion was emplaced within an intracontinental rift environment and is coeval with Jurassic flood basalts and diabase sills of the Ferrar Group of the Transantarctic Mountains (Ford & Kistler 1980, Ford & Himmelberg, in press). The intrusion comprises some 8 to 9 km of cumulate stratigraphy, of which only a total of 3 to 4 km is exposed above continental ice sheets. Because the Sallee Snowfield covers the middle portion of the stratigraphic succession, cumulates of the intrusion are ascribed to the lower Dufek Massif or upper Forrestal Range sections (Figs. 1, 2). Based on regional geophysical surveys, the areal extent of the intrusion is more than 50,000 km^2 (Behrendt *et al.* 1974, 1981); only the Bushveld Complex is possibly larger. Among the stratigraphically lowest cumulates exposed in the intrusion are plagioclase-rich rocks, which indicates that a substantial thickness of the lowermost mafic and, presumably, ultramafic cumulates is covered by ice.

The layered rocks of the Dufek intrusion are chiefly gabbroic cumulates that contain minor interlayers of anorthosite, pyroxenite, and magnetitite; the intrusion is capped by a layer of granophyre. We follow the nongenetic terminology of Irvine (1982) in our description of layered gabbros of the Dufek intrusion, and use the terms melagabbro, gabbro, leucogabbro, and anorthosite for plagioclase–pyroxene cumulates with respective modal plagioclase contents of, <40, 40–60, 60–75, and >75%; representative modes are given in Table 1.

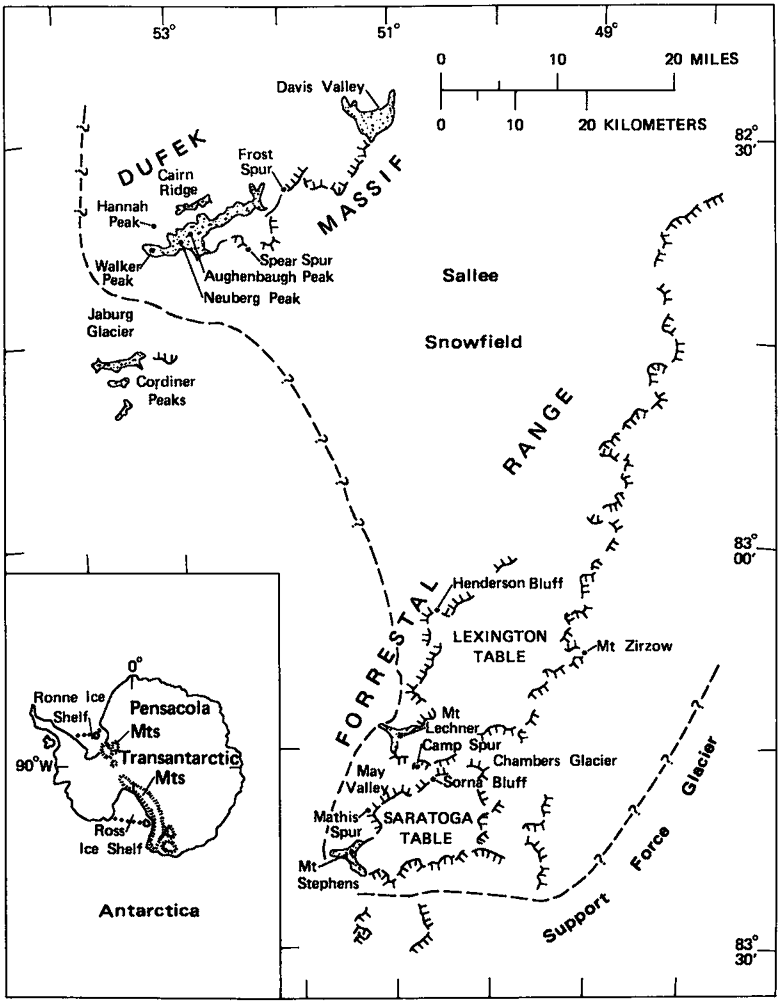

FIG. 1. Index map of the northern Pensacola Mountains showing major outcrops (stippled), localities mentioned, and southern limit of the Dufek intrusion (heavy dashed line) under ice shelves and glaciers, as inferred from geophysical surveys (Behrendt *et al.* 1981).

Many aspects of the layering, mineralogy, and petrology are similar to those in other layered intrusions (Wager & Brown 1968, Parsons 1987). Extensive descriptions of the geological setting, stratigraphy, geochronology, mineralogy, and petrology of the intrusion are found in Ford (1970, 1976), Ford & Kistler (1980), and Ford & Himmelberg (in press).

Apatite is a common accessory mineral and an intermittent cumulus phase in the Dufek intrusion, as in many other layered mafic intrusions (Wager & Brown 1968). Cumulus apatite forms when concentrations of phosphorus reach saturation levels in residual melts, typically late in the evolution of the fractionating magma. Its appearance is of such significance as, for example, to mark the base of Upper Zone c in the Bushveld Complex and the base of Upper Zone b in the Skaergaard intrusion. Mineral phases such as plagioclase and pyroxene, which may be cumulus throughout a stratigraphic section, typically are analyzed in studies of cryptic layering to monitor variations in mineral and magma chemistry, yet the fractionation of Cl, F, H_2O, P, and *REE*s may be best addressed by study of apatite. Variation in apatite chemistry has been documented for several well-known bodies of layered gabbro, including the Skaergaard intrusion (Nash 1976, Brown & Peckett 1977) and the Stillwater and Bushveld complexes (Boudreau *et al.* 1986, Boudreau &

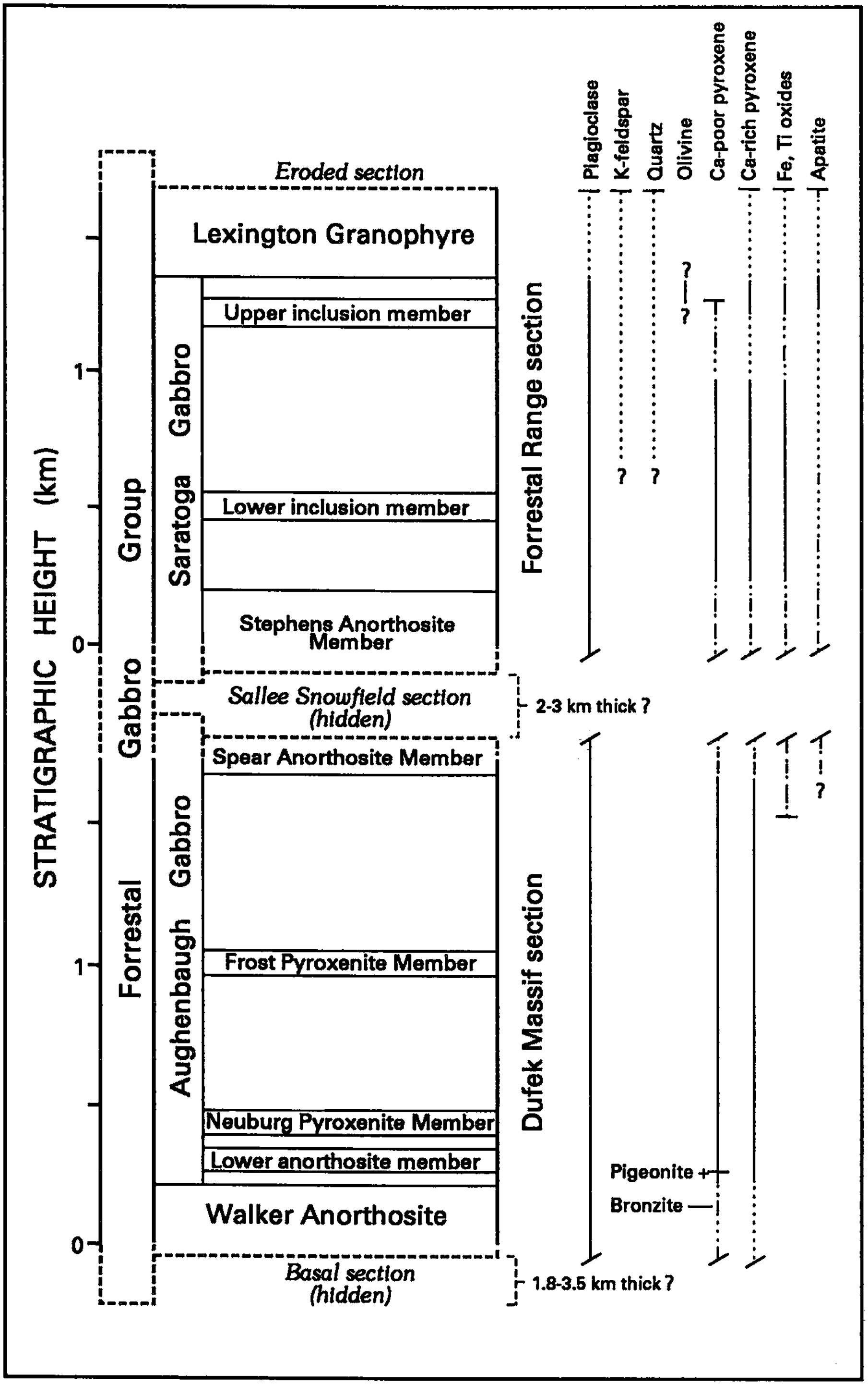

FIG. 2. Rock-stratigraphic nomenclature and generalized range of minerals in the Dufek intrusion (concealed parts of stratigraphic column dashed). Cumulus minerals, solid lines; postcumulus and noncumulus minerals, dotted lines. In places, cumulus ranges too small to show at this scale. Pigeonite +, lowest cumulus pigeonite; Bronzite, cumulus "bronzite". Uncertainties queried. Adapted from Ford (1976) and Ford & Himmelberg (in press).

TABLE 1. MODES OF REPRESENTATIVE CUMULATES OF THE DUFEK INTRUSION

Rock type Sample no.	Anorthosite 78R3N	Leucogabbro 182Fc	Gabbro 160Fa	Melagabbro 78B19N
Plagioclase	79.0	64.8	41.5	26.7
Pyroxene	9.0	21.7	46.7	53.6
Fe, Ti oxides	2.0	2.0	6.3	10.4
K-feldspar	2.7	6.2	0.2	2.5
Quartz	6.9	4.3	0.9	2.0
Apatite	0.4	1.0	4.4	4.8
Total	100.0	100.0	100.0	100.0

McCallum 1989). Other mineralogical studies on the Dufek intrusion, including electron-microprobe analyses of plagioclase (Abel *et al.* 1979, Haensel *et al.* 1986), pyroxenes (Himmelberg & Ford 1976), and Fe,Ti-oxide minerals (Himmelberg & Ford 1977), have shown both regular and irregular chemical variations with stratigraphic height.

This report follows up on that of Drinkwater *et al.* (1986) and presents petrographic descriptions, modal analyses, and results of chemical analyses of apatite as part of a continuing study of the mineralogy of the Dufek intrusion. Apatite abundances were determined by thin-section modal analysis; more than 1300 points were counted for 45 gabbroic rocks and 1000 counts for 16 granophyre samples. A suite of 25 samples was chosen for electron-microprobe analysis by a search of more than 1000 thin sections representing all exposed rock-types and stratigraphic parts of the intrusion in which apatite occurs.

Apatite grains were analyzed using an ARL–SEMQ electron microprobe with an accelerating voltage of 15 kV and a sample current of 25 nA on brass. Reported data typically represent averages for 2 to 4 grains on which 4 to 8 points were occupied for 10-second-count intervals. Standards were as follows: Ca, F, and P, Wilberforce apatite; Fe and Si, Kakanui hornblende; Cl, a natural sodalite (6.82 wt.% Cl); Ce and La, glass R236 (Roeder 1985); and Y, glass *REE*3 (Drake & Weill 1972). Analyses were not attempted for Sr because of low levels found by isotope dilution and because Watson & Green (1981) showed that partitioning of Sr in apatite is insensitive to changes in melt composition and temperature. Data were reduced by the method of Bence & Albee (1968), using the correction factors of Albee & Ray (1970).

In order to more completely document apatite chemistry, separates of cumulus and postcumulus apatite (Fig. 3) were obtained for instrumental neutron activation analysis (INAA) from typical samples of the Saratoga Gabbro (SG; Fig. 2). After initial concentration in heavy liquids, the two separates were cleansed of Fe-oxide films by heating for 15 min. at 75–80°C in a stirred mixture of 10 mL of 0.3 M Na citrate and 1.25 mL of 1 M $NaHCO_3$. After further purification by passage through a Frantz isodynamic separator at maximum current and low-angle settings, the separates were hand-picked under a binocular microscope, at 120 to 250 × magnification. Hand-picking removed a minor proportion of composite grains and grains containing infilled cavities.

STRATIGRAPHIC DISTRIBUTION

Apatite is found in the uppermost cumulates of the Dufek Massif section (the Spear Anorthosite Member, SpAM; Fig. 2) and in most rocks of the Forrestal Range section; modal data for apatite are presented in Tables 2, 3, and 4. Because of relatively high proportions of postcumulus minerals, most apatite-bearing rocks of the Dufek intrusion can be classified as mesocumulates (orthocumulates in the case of some anorthosites) according to Irvine (1982). Isomodal layers of pyroxenite and magnetitite may be true adcumulates, but apatite is rarely found in them. In fact, apatite is conspicuously absent in magnetite cumulates and magnetite-rich layers (anomalous amounts of apatite typically occur just above magnetite-rich layers). Only the gabbroic cumulates at the top of the SG contain both apatite (2–5 vol.%) and magnetite (4-11 vol.%) in significant amounts. This relation contrasts with the close association of apatite with magnetite found by Grobler & Whitfield (1970) and Reynolds (1985) in the Bushveld Complex. Although the first significant appearance of postcumulus apatite, near the base of the SpAM, also roughly correlates with the first appearance of cumulus Fe,Ti-oxide minerals (Ford 1976), correlation between the two is uncertain.

Stephens Anorthosite

Early-postcumulus apatite and large abraded and embayed apatite grains commonly occur in minor amounts in the basal anorthositic layers of the cyclic units of the Stephens Anorthosite Member (SAM; Drinkwater *et al.* 1986, Fig. 2). Apatite is most abundant (approximately 1 vol.%) in the lowermost part of these layers, decreases irregularly upward to about 0.1 vol.%, and falls below 0.1 vol.% in the gabbroic portions of the cyclic units. Early-postcumulus apatite occurs as small, discrete euhedral grains and clusters of grains that lie within postcumulus quartz, K-feldspar, biotite, or pyroxene, and may be engulfed or partly engulfed by postcumulus overgrowths of plagioclase (Figs. 4d, 5a). Clustered apatite grains may show a common crystallographic orientation; some contain infilled cavities (*e.g.*, 78R7P and 78R7N, Table 5). The abundance of apatite decreases upward within each cyclic unit and in the SAM overall; however, in the upper portions of the anorthosite layers and in the intervening gabbros, granular, late-postcumulus apa-

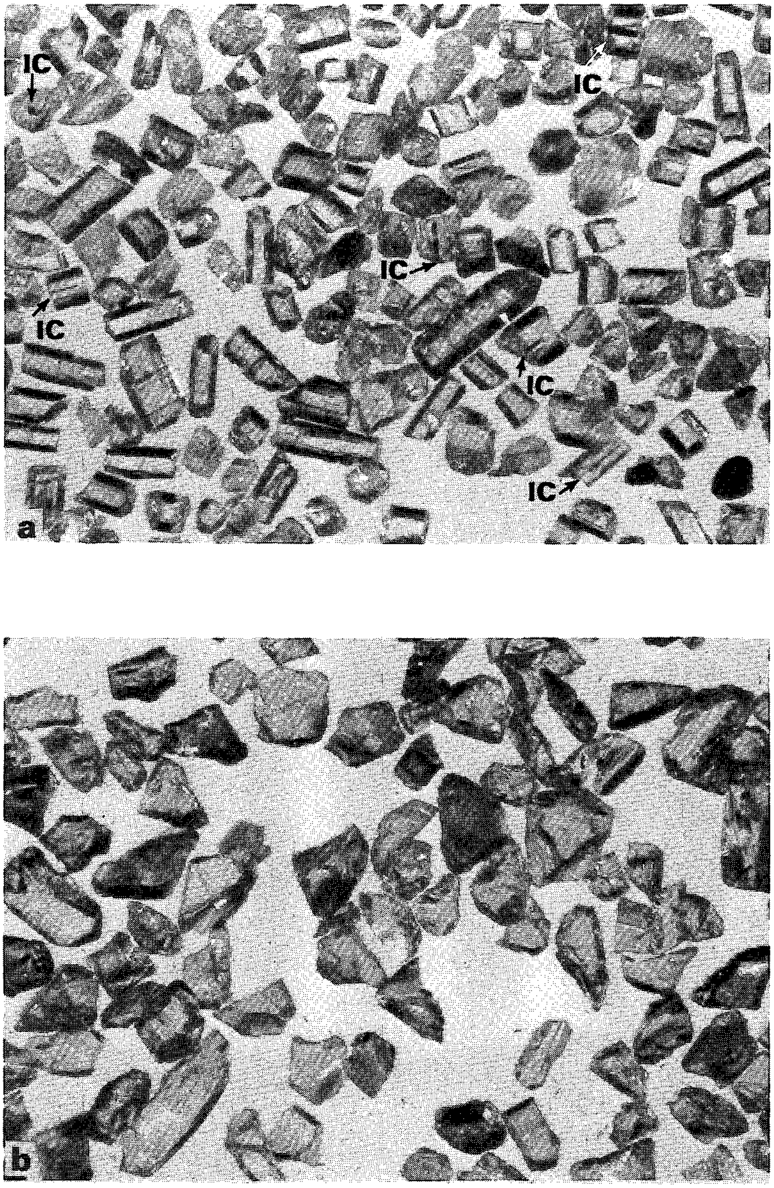

FIG. 3. Photomicrographs of apatite separates under coincident reflected and transmitted light (–60 + 300 US Standard mesh; width of each field is 4.3 mm). (a) Cumulus apatite grains with typical euhedral forms. IC, infilled cavity. Gabbro sample 160Fa of the Saratoga Gabbro. (b) Late-postcumulus (intercumulus) apatite grains with equant anhedral shapes. Anorthosite sample 182Fc of the Saratoga Gabbro.

tite becomes proportionally more conspicuous. Abundance of postcumulus apatite correlates with relative amounts of the late-postcumulus minerals quartz, K-feldspar, and biotite, estimated for the SAM to constitute <5 vol.% in gabbroic cumulates, >5 vol.% in leucogabbro and anorthosite, and 8 to 15 vol.% in the basal parts of anorthosite layers.

Unusual concentrations of abraded apatite consistently occur at the base of anorthosite layers just above magnetite troughs, but are rarely found within magnetite-rich cumulates. This large subhedral, corroded and abraded apatite, found in anorthositic and some leucogabbroic cumulates, may be recirculated cumulus apatite deposited by current activity.

Transitional zone

The Upper inclusion member (Uim) and SG above the Lower inclusion member (Lim) show transitional occurrence of postcumulus and cumulus apatite. Abundant cumulus apatite occurs in thin layers in the uppermost part of this zone, just below the Uim and within the Uim. Euhedral early-postcumulus apatite grains and anhedral late-postcumulus apatite grains (as much as 1 mm across in anorthosite) commonly occur in Transitional zone cumulates. Large subhedral apatite grains (as much as 2 mm across and 4 mm long; Fig. 4e) similar to, but more conspicuous than, those described in the SAM, also are present. These corroded, abraded, and fractured grains are stouter in shape (apparent length-to-breadth, L/B, ratios less than 10) than cumulus or early-postcumulus apatite grains, are typically clustered, and occur chiefly in coarse- to very-coarse-grained (10–25 mm) anorthositic or leucogabbroic cumulates that contain abundant postcumulus quartz and K-feldspar. The stubby habit of these large apatite grains may reflect prolonged equilibrium crystallization in the parent magma, and their embayed and corroded forms indicate later resorption in an undersaturated environment; both features can most readily be explained by extended recirculation in the magma.

TABLE 2. MODAL ABUNDANCES AND LENGTH/BREADTH RATIOS FOR CUMULUS APATITE FROM UPPERMOST GABBROS OF THE DUFEK INTRUSION

Sample no.	Unit or member	Modal % apatite	Max L/B#	Avg L/B	Meters below LG*
78B19B	SG**	1.6	10	10	2.5
78B19D	" **	2.0	8	--	5
78B19E	" **	1.4	14	--	7.5
78B19F	" **	1.6	11	12	12.5
78B19G	" **	1.5	--	--	17.5
78B19H	" **	1.8	11	--	22.5
78B19J	"	3.5	12	12	32.5
78B19K	"	2.6	20	17	40
78B19L	"	3.1	14	14	45
78B19M	"	4.0	13	--	50
78B19N	"	5.1	25	25	55
78B19O	"	5.3	34	27	60
78B19P	"	1.8	12	10	65
78B19Q	"	1.9	12	11	70
78B19R	"	1.8	14	--	75
78B19S	"	3.2	12	--	80
78B19T	"	1.9	15	16	85
78B19U	"	4.3	13	13	90
78B19V	"	3.2	21	16	95
162Fd	"	0.9	--	--	0
162Fe	"	1.2	--	--	10
161Fa	"	2.5	17	--	37
160Fa	"	4.6	16	16	55
158Fa	"	2.5	--	--	77
172Fa	"	5.6	16	--	217
69Fa	Uim	5.0	14	21	125

\# Ratio for longest grain measured.
* Distances discontinuous because of different sections represented.
** Noncumulate diorite and quartz diorite.

TABLE 3. MODAL ABUNDANCES AND LENGTH/BREADTH RATIOS FOR POSTCUMULUS APATITE FROM THE DUFEK INTRUSION

Sample no.	Unit or member	Rock type#	Modal % apatite	Max L/B*	Avg L/B	Meters below LG**
189Fa	SG	LG	0.50	9	--	412
184Fa	"	LG	0.10	--	--	549
190Fd	"	A	0.75	11	10	366
181Fa	"	A	1.00	--	--	240
182Fc	"	LG	1.00	--	--	225
70Fb	Uim	G	0.99	--	--	177
74Fa	SAM	A	0.73	7	6	1281
75Fe	"	A	0.48	--	--	1250
99Ff	"	LG	0.30	--	--	1280
94Ff	"	LG	0.40	--	--	1100
78R3B	"	G	0.20	--	--	–
78R3C	"	LG	0.30	20	--	–
78R3D	"	A	0.60	--	--	–
78R3G	"	LG	0.15	--	--	–
78R3H	"	LG	0.25	--	--	–
78R3I	"	A	0.20	16	--	–
78R3N	"	A	0.35	--	--	–
259Fc	SpAM	A	0.33	--	--	1500

\# A, anorthosite; G, gabbro; LG, leucogabbro.
* Ratio for longest grain measured.
** Distances discontinuous because of different sections represented.

TABLE 4. MODAL ABUNDANCES AND LENGTH/BREADTH RATIOS FOR APATITE FROM THE LEXINGTON GRANOPHYRE

Sample no.	Modal % apatite	Max L/B#	Avg L/B	Meters above SG*
313Fa	1.2	--	--	1.5
314Fa	0.2	44	31	84
315Na	0.4	33	--	106.5
316Fa	0.3	--	--	164
317Na	0.2	58	50	232
162Fa	1.2	40	--	1
162Fc	0.7	--	--	2
162Fb	0.5	24	--	4
163Fa	0.5	50	--	25
164Fa	0.5	--	--	55
165Fa	0.5	--	--	70
65Fb	0.8	25	24	35
64Fa	0.4	--	--	86
63Fb	0.5	30	27	125
62Fa	0.1	--	--	202

\# Ratio for longest grain measured.
* Distances discontinous because of different sections represented.

Uppermost Saratoga Gabbro

Cumulus apatite is most abundant in the 65-m-thick unit of gabbroic cumulates at the top of the SG (Fig. 2, Table 2; also Drinkwater *et al.* 1986, Fig. 1). As much as 5.3 vol.% apatite is found in the well-laminated quartz-bearing melagabbros of the middle part of this section, and most of these cumulates contain more than 2 vol.% apatite. The 25-m-thick unit of noncumulate diorite and quartz diorite above the cumulates contains between 1.4 and 2 vol.% apatite.

Cumulus apatite occurs as elongate, euhedral prismatic grains that lie in the plane of lamination of plagioclase (Fig. 4a) and in some sections shows preferred alignment in that plane; average diameters range from 0.05 to 0.2 mm (maximum 0.5 mm) and lengths from 2 to 3 mm. L/B ratios range from 12 to 34 and average about 16. Cumulus apatite occasionally occurs in clusters or is concentrated along layers, but typically shows uniform distribution on a thin-section scale. Thin infilled cavities are not uncommon (Fig. 3a).

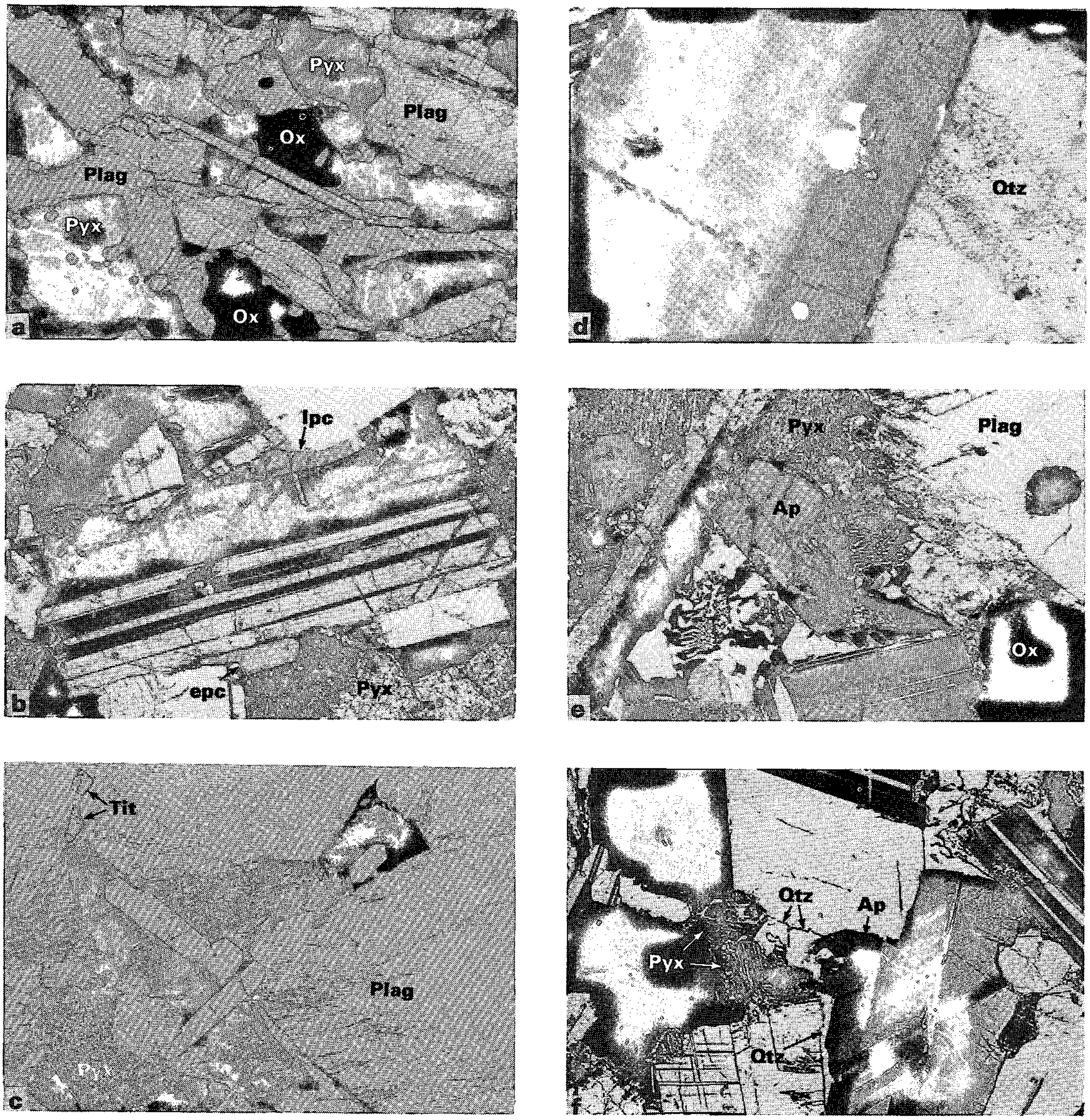

FIG. 4. Photomicrographs of typical occurrences of apatite in rocks of the Dufek intrusion (Ap, apatite; epc, early-postcumulus apatite; lpc, late-postcumulus apatite; Ox, Fe,Ti-oxide minerals; Plag, plagioclase; Pyx, pyroxene; Qtz, quartz; Tit, titanite). Except for (d), in which the width of field is 2.3 mm, field widths are 3.7 to 4.9 mm. (a) Cumulus apatite in laminated melagabbro of the uppermost Saratoga Gabbro. Note numerous cross-sections and prismatic elongate sections of apatite, which lie in the plane of lamination. Length of elongate apatite grain in center of photo is 1.5 mm. Sample 78B19O, plane light. (b) Early- and late-postcumulus apatite in laminated gabbro below the Upper inclusion member. Typical late-postcumulus apatite at top center fills void between cumulus plagioclase grains. Subhedral early-postcumulus apatite grain at bottom center exhibits a late-postcumulus extension between cumulus plagioclase grains. Sample 72Fa, crossed nicols. (c) Euhedral early-postcumulus apatite grains clustered within late-postcumulus pyroxene in anorthosite of the Stephens Anorthosite Member. Note two small grains of titanite and broad alteration rims on plagioclase grains. Sample 78R7A, plane light. (d) Cross-sections of three grains of euhedral apatite enclosed by overgrowth of plagioclase. Largest grain is 0.1 mm across. Leucogabbro sample 78R3B of the Stephens Anorthosite Member, crossed nicols. (e) Large, fractured subhedral apatite grain enclosed in quartz - K-feldspar granophyre. Grain (1.7 mm long) shows abraded margins and corrosion, suggesting a cumulus, detrital origin. Sample 181Fa of leucogabbro below the Upper inclusion member, crossed nicols. (f) Apatite grain (0.8 mm across) showing well-formed, early-postcumulus faces where overgrown by plagioclase, and irregular late-postcumulus intergrowth with quartz and pyroxene. Gabbro sample 78R7V of the Stephens Anorthosite Member, crossed nicols.

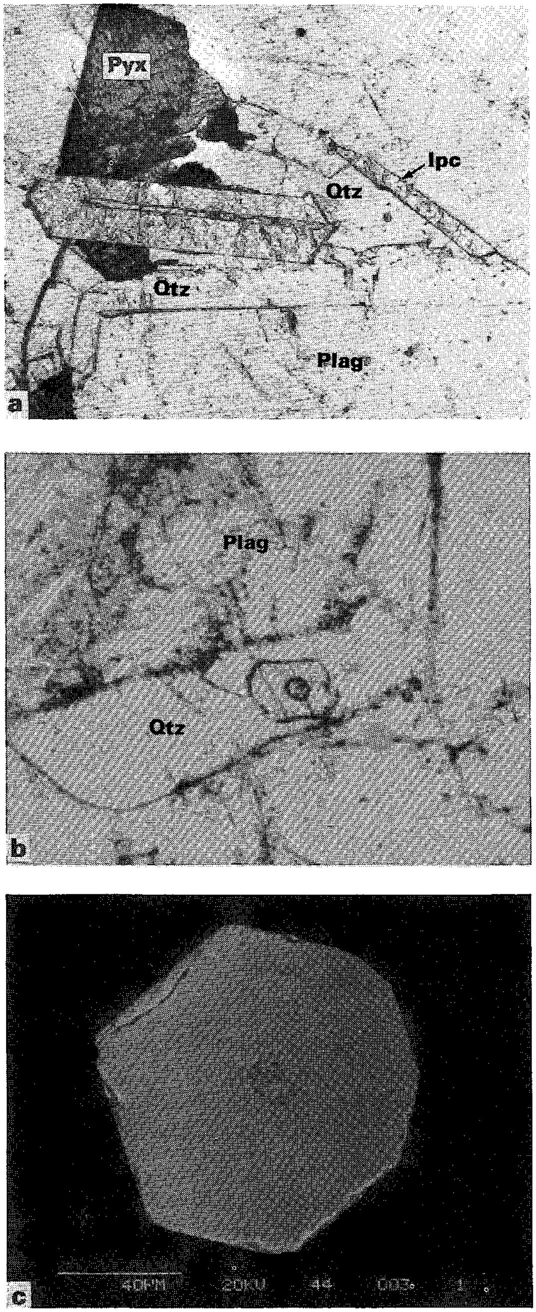

FIG. 5. Photomicrographs of apatite containing infilled cavities. (a) Euhedral early-postcumulus apatite grain (0.65 mm long) and anhedral late-postcumulus apatite in interstice with postcumulus quartz and pyroxene. Euhedral grain partly engulfed by postcumulus overgrowth of plagioclase. Leucogabbro sample 78F15A of the Stephens Anorthosite Member, crossed nicols. (b) Cross-section of apatite grain (0.2 mm across) containing central filled cavity. Apatite host is quartz, surrounded by cumulus plagioclase. Sample 78R3D from anorthosite of the Stephens Anorthosite Member, plane light. (c) Back-scattered electron image of cumulus apatite grain showing cross-section of hexagon-shaped filament composed of lepidomelane and smectite (see Table 5). Edges of infilled cavity are parallel to edges of apatite grain. Sample 160Fa from main cumulus-apatite horizon of the Saratoga Gabbro.

Lexington Granophyre

Apatite occurs in much lower abundance (0.2–1.2 vol.%) in the capping Lexington Granophyre (LG) than in rocks of the underlying SG. It occurs as acicular euhedral primocrysts that are more abundant near the base of the LG and decrease in abundance upward. The acicular habit of apatite in the LG is shown by L/B ratios ranging from 24 to 50. Most apatite grains measure from 0.02 to 0.04 mm across; the largest grains, found near the base of the granophyre, are as broad as 0.1 mm. Apatite is commonly found within the granophyric groundmass, across quartz - K-feldspar grain boundaries, and within these minerals; it also occurs as inclusions in augite (or amphibole and biotite reaction rims on augite) and in plagioclase microphenocrysts. Other accessory minerals found in the LG are allanite, zircon, and titanite.

WHOLE-ROCK P_2O_5 CONTENTS AND THE BEHAVIOR OF P

Students of layered mafic intrusions have devoted much attention to the stratigraphic variation of P content within these bodies since Wager & Deer (1939) observed that, because it is in very low concentration in cumulus silicates, P content can be correlated with content of mesostasis (in the sense of Henderson 1970) in cumulates. As noted by subsequent investigators, refinement of this approach is complicated by (1) measurable concentrations of P in cumulus minerals (*e.g.*, Henderson 1968, Campbell 1987), (2) typically increasing P content in successive fractions of residual melt, (3) common lack of knowledge of the composition of the parental melt, and (4) such complexities as influx of new magma. Recognizing these constraints, Wager (1963), Henderson (1970), Morse & Allison (1986), Campbell (1987), and Cawthorn & Walsh (1988) have made notable contributions toward the utilization of P contents to better understand layered mafic cumulates.

The roughly 100 determinations of the whole-rock concentration of P available to us, combined with some 20 analyses for P in plagioclase separates, provide a base for cautious discussion of the behavior

TABLE 5. REPRESENTATIVE COMPOSITIONS OF LEPIDOMELANE AND SMECTITE FILAMENTS IN APATITE CRYSTALS (WT%)

	182Fc					78R7P	78R7N	78R19B
	4A	2B	2A	2E	2E			
SiO_2	36.0	34.9	37.4	34.6	38.4	36.3	35.3	40.4
Al_2O_3	12.7	14.0	13.0	12.8	6.86	11.3	9.16	8.51
FeO^T	29.9	35.0	29.4	31.9	34.7	30.6	28.0	24.4
MgO	6.15	2.23	5.20	5.50	5.68	3.15	9.19	9.05
CaO	0.48	0.75	1.06	0.57	1.12	2.19	2.09	1.23
Na_2O	0.10	0.08	0.18	0.07	0.40	0.23	0.79	0.04
K_2O	8.07	7.22	6.09	7.46	1.46	3.07	0.85	0.11
TiO_2	0.07	0.05	0.04	0.02	0.02	0.08	0.02	0.08
MnO	0.13	0.21	0.18	0.18	0.33	0.07	0.06	0.06
Total	93.6	94.4	92.6	93.1	89.0	87.0	85.5	83.9
Si	2.942	2.889	3.035	2.876	3.268	3.130	3.045	3.384
Al	1.058	1.111	0.965	1.124	0.688	0.870	0.931	0.616
Al	0.165	0.255	0.279	0.130	--	0.278	--	0.224
Ti	0.004	0.003	0.002	0.001	0.001	0.005	0.001	0.005
Fe^{2+}	2.044	2.423	1.996	2.218	2.470	2.207	2.020	1.709
Mn	0.009	0.015	0.012	0.013	0.024	0.005	0.004	0.004
Mg	0.749	0.275	0.629	0.682	0.721	0.405	1.182	1.130
(M1-M2)	2.971	2.971	2.919	3.044	3.216	2.900	3.183	3.072
Ca	0.042	0.067	0.092	0.051	0.102	0.202	0.193	0.110
Na	0.016	0.013	0.028	0.011	0.066	0.038	0.132	0.006
K	0.841	0.762	0.631	0.791	0.157	0.338	0.094	0.012
(A)	0.899	0.842	0.751	0.853	0.325	0.578	0.419	0.128

of P in the Dufek intrusion. Determination of P in plagioclase was by precision XRF, accurate to 0.003 wt.% P_2O_5, based on comparison with three feldspar standards. P_2O_5 content in six plagioclase separates from the Dufek Massif section is uniformly 0.02 wt.% and in 15 separates from the Forrestal Range section is uniformly 0.03 wt.%. Based on Henderson's data (1968) for Bushveld minerals, P concentrations in cumulus pyroxene may be somewhat less. Concentrations of whole-rock P were determined by the colorimetric, molybdivanadophosphate method, considered to provide data fully adequate for the purposes of our discussion. P_2O_5 contents range from 0.02 to 0.07 wt.% and average 0.04 wt.% in 24 cumulates representing some 1800 m of the Dufek Massif section below the SpAM (Ford, unpubl. data); apatite is rarely seen in these rocks. Similar whole-rock concentrations of P_2O_5 are reported for the Skaergaard intrusion (Wager 1960), the Bushveld Complex (Henderson 1968, Cawthorn & Walsh 1988), and the Jimberlana Intrusion (Campbell 1987).

Notably higher concentrations of P_2O_5, typically 0.13 to 0.18 wt.%, are present in the typical postcumulus-apatite-bearing cumulates of the Forrestal Range section; as seen in Figure 6, there is no discernable change in P_2O_5 content of these rocks with stratigraphic height. Because whole-rock P_2O_5 contents in his Skaergaard samples did not increase with stratigraphic position, as was expected from calculations which show that P should rise in fractionated melts, Wager (1963) concluded that the trapped interstitial-liquid component in the rocks diminished with stratigraphic height. He considered this conclusion to be confirmed by thin-section observations. McBirney (1989) has recently called Wager's interpretation into question, and we find no indication from thin sections of Forrestal Range samples that trapped interstitial liquid content is a significant variable. Morever, indications of magma replenishment in the Dufek intrusion render questionable any calculation of P buildup in residual-melt fractions. If three samples of anorthositic cumulates containing 0.31, 0.50, and 0.63 wt.% P_2O_5 are excluded from consideration, P_2O_5 contents of 39 remaining samples range from 0.10 to 0.24 wt.%. This sample population can be split into roughly equal numbers of well-interspersed samples of melagabbro, gabbro, leucogabbro, and anorthosite, with average P_2O_5 contents of 0.13, 0.17, 0.16, and 0.18 wt.%, respectively. Based on comparison with the P_2O_5 contents of Dufek Massif cumulates, at least 70 to 80% of the P in these cumulates may be contained in apatite.

The sudden and rapid increase in P_2O_5 content shown in Figure 6 corresponds to the appearance of abundant cumulus apatite, about 450 m below the erosional top of the intrusion. However, the first occurrence of more than 1 vol.% cumulus apatite is found near the base of the Uim, approximately 100 m below the level of the main cumulus-apatite horizon. Aborted, early occurrence of cumulus apatite also has been noted in the Bushveld Complex (Cawthorn & Walsh 1988, p. 83). P_2O_5 and apatite contents decrease significantly in the overlying noncumulate diorite and LG, although apatite is still present in amounts greater than those found in the layered rocks below the uppermost cumulates of the SG.

Cumulates of the Forrestal Range section appear to be uniquely rich in P. A few scattered samples with comparable P content have been analyzed by Henderson (1968) for the Bushveld Complex and Campbell (1987) from the Jimberlana Intrusion, but no known sequence of samples is as rich in P. Henderson (1968) suggested that a greater predominance of adcumulates or near-adcumulates may characterize the early stages of fractionation in the Bushveld Complex, accounting for the lower contents of P in those rocks. However, because a significant thickness of lowermost cumulates of the Dufek intrusion is unexposed, the cumulates of the Dufek Massif section do not represent early fractionation. Morever, thin sections reveal no significant distinction between the textures of cumulates from the Forrestal Range and those from the Dufek Massif.

That P contents in the lower 1300 m of the Forrestal Range section (Fig. 6) uniformly average four times those in Dufek Massif section is a significant petrological problem, beyond resolution here. Wager's Skaergaard data (1963, Fig. 8) show that it is not unique that P contents in Forrestal Range cumulates are essentially constant up to the onset of cumulus apatite precipitation, but why are they so

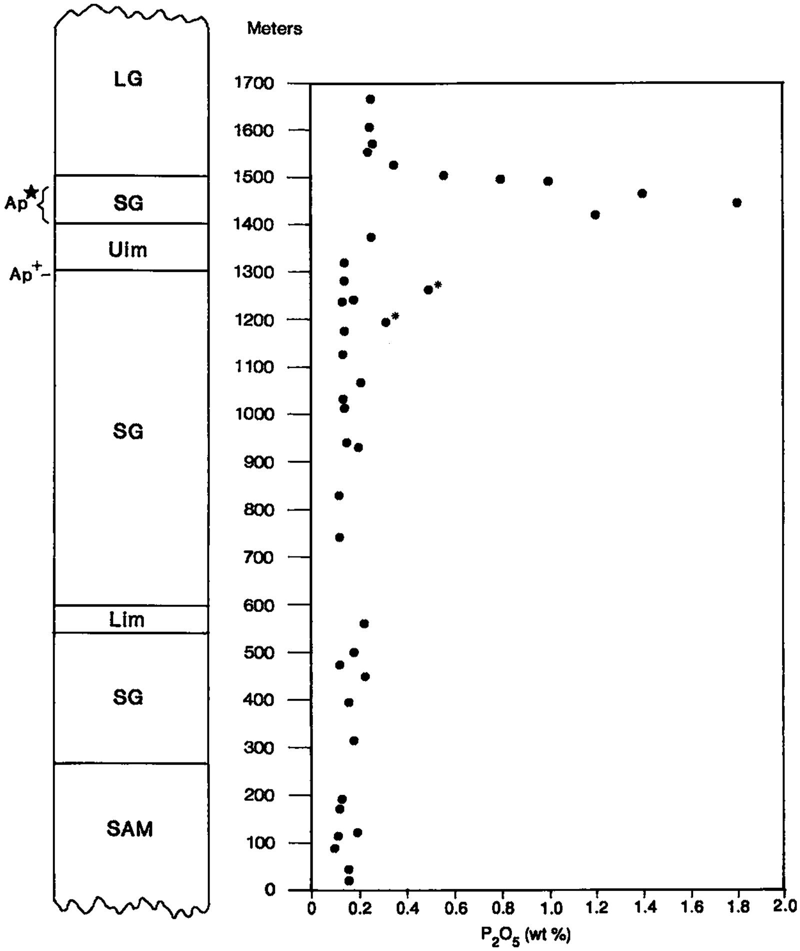

FIG. 6. Variation of P_2O_5 content with stratigraphic height in the Sorna Bluff traverses of the Forrestal Range section. Ap$^+$, first appearance of abundant cumulus apatite. Ap*, main cumulus-apatite horizon. Two data points with stars are from the Camp Spur and Mt. Lechner traverses (Fig. 1). See Fig. 1 for localities and Fig. 2 for nomenclature of zones.

high? It is unfortunate that the cumulate sequence between the Dufek Massif and Forrestal Range sections is covered by the Sallee Snowfield, for it appears that introduction of a major pulse of P-enriched magma may best explain the contrast. Support for a major shift in magma composition subsequent to deposition of the Dufek Massif section is provided by Ford *et al.* (1986), who reported distinctly different Rb/Sr ratios and oxygen-isotopic characteristics for the Dufek Massif and Forrestal Range sections. Evidence for large-scale replenishment of the Dufek magma chamber at the level of 500 m above the base of the Forrestal Range section is given by strong reversals in Fe/(Fe + Mg) ratios in cumulus pyroxene (Himmelberg & Ford 1976), and Ab/(An + Ab) ratios in cumulus plagioclase (Abel *et al.* 1979, Haensel *et al.* 1986), as well as Al and V contents of "ilmeno-magnetite" (Himmelberg & Ford 1977). Thus, an earlier replenishment event would not be unique. Campbell (1987, p. 41) raised the alternative possibility that a magma chamber could be zoned, with increasing P content upward.

Consideration of the P contents of the gabbros that contain cumulus apatite and of the overlying granophyre is conveniently done in the context of the review and generalizations of Cawthorn & Walsh (1988), who discussed the petrologically comparable Bushveld Complex. They concluded that cumulus apatite can be expected to appear at 1000–1050°C from melts containing 50 to 55 wt.% SiO_2 and 1.0 to 1.9 wt.% P_2O_5, and quoted Wager (1960) as suggesting a P_2O_5 content of 0.4 wt.% for the end stages of differentiation. Comparable values obtained by Helz (1987) from study of core from the Kilauea Iki lava lake are 1065 + 10° C for commencement of apatite crystallization from melts containing 57 to 58 wt.% SiO_2 and about 1.45 wt.% P_2O_5. Forrestal Range samples 161Fa and 162Fd (Table 2), chosen as being relatively free of cumulus Fe,Ti-oxide minerals, contain, respectively, 49.8 and 50.3 wt.% SiO_2 and 1.4 and 0.80 wt.% P_2O_5. An average P_2O_5 content of 1.24 wt.% is representative of the 80-m-thickness of cumulus-apatite-bearing gabbros represented by the sample series 158 through 162 in Table 2. If we take this value and the range of P_2O_5 contents of 0.13 to 0.18 wt.% that characterizes the cumulates just below the point at which apatite saturation occurs, and loosely follow Cawthorn & Walsh (1988), the interstitial-melt content in those cumulates can be estimated to have been 10 to 15% (neglecting the P in the cumulus minerals). These values are notably greater than those calculated by Cawthorn & Walsh for the Bushveld Complex and compare favorably to contents of 5 to 15 modal % of late-postcumulus minerals (quartz, K-feldspar, and biotite) measured in underlying cumulates of the SG and SAM. Eight samples of granophyre contain from 0.24 to 0.56 wt.% P_2O_5. An average of these values would be misleading, as there is an excellent negative correlation between SiO_2 and P_2O_5 contents, extending from 0.55 wt.% P_2O_5 at 60 wt.% SiO_2 to 0.25 wt.% P_2O_5 at 69 wt.% SiO_2. In comparison, Wager's (1960, Table 4) residual value of 0.40 wt.% P_2O_5 pertains to a sample from zone L. UZc containing 55 wt.% SiO_2.

PETROGRAPHIC DESCRIPTION

Apatite from the Dufek intrusion has optical and physical characteristics typical of igneous fluorapatite; moderately high relief, very low birefringence (0.002–0.004), specific gravities between 3.17 and 3.20, and diffraction spacings of 2.80 (100), 2.70 (60), 2.77 (55), and 3.44 (40). Indices of refraction ($\pm$ 0.002) for apatite 160Fa are $\epsilon = 1.632$, $\omega = 1.635$, and for apatite 182Fc, $\epsilon = 1.631$, $\omega = 1.634$.

We distinguish four types of apatite; 1) cumulus, 2) early postcumulus, 3) late postcumulus, and 4) noncumulus primocryst. These designations, based on morphology, grain size, and textural relations, are substantiated by mineral chemistry. Figure 3 gives an indication of the difference in morphology between typical cumulus and late-postcumulus apatite. The results of modal analyses and grain-size measurements are summarized in Tables 2 through 4. Cumulus apatite is recognized by its elongate prismatic habit (L/B ratios of 12–34) and its alignment in the plane of lamination of plagioclase (Fig. 4a). Cumulus apatite grains range from 0.05 to 0.2 mm in cross section, with lengths between 1 and 3 mm.

Large, subhedral apatite grains occurring in coarse-grained anorthosites of the SG are tabular to subequant prismatic in habit and may be as long as 4 mm and as broad as 1 mm (Fig. 4e). These apatite grains are typically corroded, abraded, and fractured, and are interpreted to represent recycled or "detrital" cumulus apatite.

Postcumulus apatite occurs as two distinct types (Figs. 4b, 5a), both of which are part of the mesostasis. Early-postcumulus apatite grains are euhedral to subhedral and similar in form to cumulus apatite, but are generally somewhat smaller, with lower L/B ratios. They typically occur in clusters within postcumulus quartz or quartz – K-feldspar intergrowths, or less commonly within interstitial pyroxene (Figs. 4c, 5a); they may be partly to completely engulfed by postcumulus overgrowths of plagioclase (Figs. 4d, f, 5a), and are more abundant in leucogabbro or anorthosite than gabbro. Cumulus plagioclase in apatite-bearing rocks of the Dufek intrusion typically shows zoning of 2.5 to 10 mol% An, within the range of 50 to 63 mol% An (Abel *et al.* 1979, Haensel *et al.* 1986). Broad overgrowths of uniformly more sodic plagioclase (Figs. 4d, f) are interpreted to represent postcumulus growth, and the apatite grains within them, to represent early-postcumulus crystallization. Late-postcumulus apatite fills voids and forms overgrowths on early-postcumulus or cumulus apatite grains (Fig. 4b). Late-postcumulus apatite grains are identified by anhedral, more stout or irregular shapes, as controlled in part by the interstitial spaces they fill (Figs. 4b, 5a), but they may be as much as 1 mm across.

As much as 2.0 vol.% of primocrystic apatite occurs as small euhedral grains in quartz diorite of the uppermost part of the SG and as small acicular grains in the LG.

Some investigators may argue that what we interpret as early-postcumulus apatite is cumulus by the definitions of Wager & Brown (1968) or Irvine (1982). However, in cumulates below the Uim, these extremely well-formed grains contrast notably in size and form with the subhedral, abraded apatite grains thought to be derived from the contemporary "bulk" magma. This interpretation supercedes that of Drinkwater *et al.* (1986), who did not recognize the paragenetic distinction between cumulus and early-postcumulus apatite. Boudreau & McCallum (1989) described euhedral apatite from the Stillwater Complex as being postcumulus and associated with interstitial quartz. Morse & Allison (1986) commented that the commonly observed capacity of apatite to grow as faceted crystals in interstitial spaces makes texture an unreliable guide to its cumulus status. Late-postcumulus apatite formed during advanced stages of crystallization from the trapped interstitial liquid. Apatite grains that in part exhibit idiomorphic boundaries and in part exhibit intergrowth relationships with postcumulus minerals (Fig. 4f) represent a transition between early- and late-postcumulus types.

A notable feature of some cumulus and early-postcumulus apatite grains is the presence of infilled cavities parallel to their *c* axes (Fig. 5), resembling the infilled "hollow" apatite described by Gardner (1972) for the Hasvik layered intrusion of Norway. Gardner thought that the infilled apatite grains contained trapped melt and considered them to be transported cumulus grains, representing rapid quenching of magma in the roof zone of the Hasvik intrusion. A small proportion of infilled apatite grains (*e.g.*, Fig. 3a) is common in the cumulus apatite population in cumulates of the uppermost SG and in several horizons in the Uim. Infilled cavities occur less frequently in early-postcumulus apatite grains in the SAM and rarely in the rest of the SG. Postcumulus occurrences of infilled apatite appear to be proportionally more common where postcumulus apatite is most abundant. For example, within the cyclic units of the SAM, infilled apatite is most notable in the lowermost layers of the anorthositic cumulates.

TABLE 6. INAA DATA FOR TWO APATITE SEPARATES (PPM, EXCEPT OXIDE VALUES IN WT%)

	160Fa		182Fc	
Al_2O_3	1.88	(4)	0.65	(6)
Ba	119	(10)	51	(16)
Co	0.91	(5)	0.75	(5)
Cr	5.8	(5)	7.1	(4)
Cs	0.12	(12)	0.06	(18)
FeO	0.30	(4)	0.30	(4)
Hf	0.15	(11)	1.8	(2)
K_2O	0.18	(35)	0.14	(35)
MgO	0.48	(13)	0.30	(16)
Mn	330	(3)	375	(2)
Na_2O	0.31	(1)	0.15	(1)
Ni	92	(4)	27	(12)
Rb	3.4	(15)	3.8	(14)
Sb	0.10	(17)	0.07	(21)
Sc	0.66	(2)	0.33	(3)
Sr	363	(5)	182	(8)
Ta	0.04	(15)	0.07	(12)
Ti	650	(20)	320	(22)
Th	11.9	(1)	7.69	(1)
U	4.16	(2)	4.15	(2)
V	0.50	(45)	1.90	(35)
Zn	84	(4)	91	(3)
Zr	579	(5)	253	(7)
La	295	(1)	498	(1)
Ce	827	(1)	1300	(1)
Nd	601	(2)	807	(1)
Sm	171	(1)	207	(1)
Eu	21.9	(1)	7.25	(1)
Gd	187	(2)	208	(2)
Tb	25.5	(1)	30.0	(1)
Tm	8.20	(3)	10.4	(2)
Yb	42.5	(2)	51.2	(2)
Lu	5.30	(2)	6.01	(2)

Analyst: James R. Budahn, U.S. Geological Survey, Denver, CO.

* Counting statistic error (in percent) calculated for the best peak from the duplicate sample splits whose averages are reported.

TABLE 7. RUBIDIUM AND STRONTIUM ABUNDANCES IN APATITE OF THE DUFEK INTRUSION

Sample no.	Unit	Rock type#	Rb (ppm)	Sr (ppm)	Rb/Sr
162Fe	SG	G	7.8	265	0.029
160Fa	"	G	5.4	313	.017
158Fa	"	G	5.2	241	.022
182Fc	"	A	2.1	203	.010
184Fa	"	LG	6.6	176	.038
84Fa	SAM	G	6.2	239	.026
99Ff	"	LG	6.4	182	.035
75Fe	"	A	6.7	177	.038
74Fa	"	A	6.1	181	.034

\# A, anorthosite; G, gabbro; LG, leucogabbro. Rubidium and strontium concentrations determined by standard isotope-dilution techniques, U.S. Geological Survey, Menlo Park; analyst, Allen Robinson. Total error, including sample inhomogeneity, <1% for Sr measurements.

During the process of purifying the two apatite separates for INAA, a significant number of cumulus apatite grains from sample 160Fa of the uppermost SG were noted to contain red-brown "filaments". In cross section, these filaments are 5 to 15 μm thick and have hexagonal to roundish outlines (Fig. 5c); they parallel the *c* axis and may occupy nearly the full length of well-formed crystals (Figs. 3a, 5a). A selection of these infilled grains was mounted in epoxy so that sections perpendicular to their *c* axes could be lapped and polished for exposure of the infilled cavities. Electron-microprobe analyses (Table 5) show that the predominant primary infilling phase is iron-rich biotite (lepidomelane), which has been partly altered to a smectite-group mineral. Aside from containing notably less Ti, the lepidomelane analyses of Table 5 are comparable to analyses 8, 10, and 11 of Table 12 in Deer *et al.* (1962). The most comparable smectite compositions of Deer *et al.* are analyses 10 and 11 of their Table 39, described as nontronite occurring in basalt. The two middle columns of Table 5 represent two parts of the end section of the filament shown in Figure 5c; the lepidomelane appears in the back-scattered electron image as a smooth surface, and the nontronite as a less bright, less coherent mass. Quartz was detected in one filament section, but data for perhaps 40% of the cavities are uninterpretable. The remaining three apparent nontronite analyses of Table 5 were made from polished thin sections containing infilled apatite grains (*e.g.*, Figs. 5a, b). Analyses of infilling material in thin section also revealed that rarely cavities contain quartz and nearly pure K-feldspar, containing less than 0.25 wt.% CaO and 0.45 wt.% Na_2O.

We suggest that the infilling phases in Dufek apatite crystallized as the crystals grew. Gardner's (1972) discussion regarding the significance of infilled apatite grains seems overly speculative. Infilling minerals could as well represent simultaneously grown phases as crystallization products from trapped melt, and magmatic overturn seems an overly dramatic cause for discontinuous cavities. S.A. Morse (pers. comm., 1989) substantiated our impression that Gardner was erroneous in visualizing infilled apatite in Kiglapait photomicrographs; none has been recognized from that intrusion. However, A.R. McBirney (pers. comm., 1989) confirmed the presence of infilled apatite grains in the Skaergaard intrusion, has identified biotite as the dominant infilling phase, and concurs with our suggestion of simultaneous crystallization. Recognition of biotite, quartz, and K-feldspar as infilling phases substantiates our argument that, in the Dufek intrusion, infillings are not trapped primitive melt.

Wyllie *et al.* (1962) showed both synthetic and natural apatite grains with hollow cores and ascribed the morphology to quenching in the presence of a liquid. Our findings call into question the premise that infilled apatite grains result only upon quenching, because quenching and apatite supersaturation may rarely be concomitant in a major layered mafic body. Hydrothermal experiments by Argiolas & Baumer (1978) produced, under specific conditions, spectacular hollow and non-terminated apatite crystals. They emphasized that, in their experience, growth of acicular (L/B ratios of 5–20) and hollow apatite crystals is not due to rapid quenching, but to a high degree of supersaturation. Infilled apatite grains in the Dufek intrusion constitute only a fraction of the total apatite population within a given specimen and show no macroscopic distinction. Because biotite stability in the magma must only be realized in special circumstances, yet biotite is the predominant infilling phase in "hollow" apatite crystals, we can only conclude that these grains represent rapid crystallization in isolated environments also characterized by supersaturation in apatite.

MINERAL CHEMISTRY

INAA data were obtained for two representative apatite separates (Table 6), and Sr and Rb abundances were measured by isotope dilution on nine apatite samples distributed throughout the Forrestal Range section (Table 7). To our knowledge, the analyses of Table 6 are the most complete available for apatite from a layered mafic intrusion. Aside from numerous electron microprobe analyses, Paster *et al.* (1974) presented results of a single INAA analysis for 9 elements for a Skaergaard apatite, Huntington (1979) presented results of three 14-element INAA analyses of Kiglapait apatite, and Roelandts & Duchesne (1979) presented results of nine INAA analyses for *REEs* in apatite from the Bjerkrem–Sogndal layered lopolith (southwestern Norway). *REE* patterns for all except the apatite suite from Kiglapait are shown in Figure 7. The three samples of cumulus apatite from Kiglapait occur in rocks that correspond to 95.0, 97.0, and 98.1% solidification of the intrusion. *REE* patterns of the apatite from Kiglapait do not evolve with percent solidification and are quite similar to the pattern for cumulus apatite from Dufek sample 160Fa, although the Eu anomalies are only 1/2 to 3/4 as large, and two of the three show relative Yb and Lu depletion. Perhaps the most informative comparison is between our data and those for apatite from the upper three (of five) macroscale rhythmic units of the Bjerkrem–Sogndal lopolith, which are interpreted to result from repeated influx of fresh magma; cumulus apatite first appears in the upper part of rhythm III. Roelandts & Duchesne (1979) analyzed three apatite separates from the upper three rhythms and, finding apatite in each to be comparable in composition, based their discussion on an average composition for each rhythm. *REE* concentrations and the magnitude of the Eu anomaly increase steadily for rhythms III through V, reaching concentrations and a *REE*-distribution pattern comparable to that for apatite 160Fa (Fig. 7). In distinction, the *HREE*s are notably lower in apatite from Bjerkrem–Sogndal, and the Eu anomaly never reaches that of apatite 160Fa. The *REE*-distribution pattern for apatite from Skaergaard sample EG4312 (Paster *et al.* 1974) is dissimilar to all other samples of apatite discussed here in reflecting notably higher *MREE* concentrations and a minimal Eu anomaly (Fig. 7). Both must stem from significantly different *REE* concentrations in the Skaergaard magma compared to those in the other magmas.

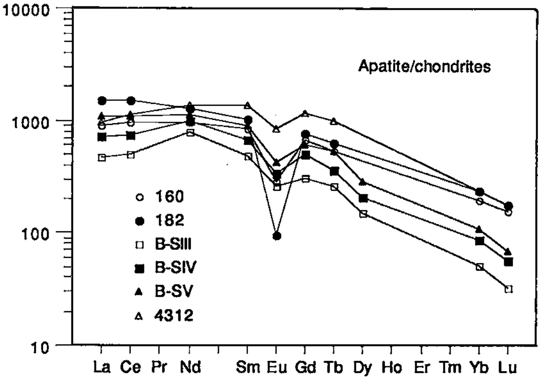

FIG. 7. Chondrite-normalized *REE* patterns (calculated with SPIDER, Wheatley & Rock 1988) for apatite in mafic intrusions. 160 and 182, the Dufek apatite fractions of Table 6. B–SIII, B–SIV and B–SV: average apatite in the upper three rhythmic units of the Bjerkrem–Sogndal lopolith (Roelandts & Duchesne 1979, Table 1). 4312, apatite from UZb of the Skaergaard intrusion (Paster *et al.* 1974, Table 2).

Higher *REE* content and a larger Eu anomaly, relative to cumulus apatite 160Fa, are consistent with the fact that apatite in sample 182Fc is postcumulus. The fact that sample 182Fc represents an anorthositic cumulate, located some 200 m lower in the section than gabbroic cumulate 160Fa, tempers con-

TABLE 8. ELECTRON-MICROPROBE DATA FOR APATITE FROM THE DUFEK INTRUSION (WT%)

Sample no.	Unit or zone	Rock type$^{\#}$	Apatite type*	F	Cl	SiO_2	FeO	Y_2O_3	Ce_2O_3	La_2O_3	P_2O_5	CaO	Ce/Y**	F/Cl**
78B18FF	LG	gg	p	3.4	0.02	0.19	0.45	0.23	0.42	0.20	40.0	55.5	1.26	315
78B18AA	"	gg	p	3.5	.01	.18	.24	.24	.42	.22	40.1	55.3	1.20	648
78B18V	"	gg	p	3.4	.02	.18	.25	.25	.43	.17	40.3	55.1	1.17	315
78B180	"	gg	p	3.5	.01	.19	.19	.24	.47	.20	40.1	55.5	1.33	648
78B18I	"	gg	p	3.1	.01	.20	.20	.25	.40	.17	40.3	55.8	1.07	574
78B18C	"	gg	p	3.0	.08	.18	.16	.25	.45	.19	40.4	55.6	1.20	72
79B19B	SG	FD	c	2.9	.13	.09	.29	.12	.08	--	41.2	55.6	0.49	41
79B19Q	"	MG	c	3.1	.09	.15	.34	.12	.07	--	41.4	54.9	0.42	63
79B19U	"	MG	c	3.3	.10	.15	.33	--	.14	--	41.5	54.7	--	61
69Fa	"	MG	c	3.4	.09	.09	.36	.12	.07	--	41.1	55.0	0.42	70
70Fa^{o}	Uim	G	pc	3.1	.21	.11	.40	.11	.21	.11	41.7	55.6	1.26	28
71Fb	SG	G	pc	3.4	.17	.11	.35	.13	.18	.08	41.2	55.4	0.95	37
72Fa	"	G	pc	3.1	.18	.09	.31	.11	.16	.07	40.6	55.2	0.98	31
191Fb^{o}	"	G	pc	2.5	.35	.13	.25	.10	.15	--	40.6	55.7	0.98	13
190Fd	"	A	c	3.2	.16	.10	.19	.15	.19	--	41.0	54.7	0.88	37
"	"	"	pc	3.1	.19	.10	.18	.17	.22	--	41.2	54.8	0.86	30
188Fa	"	A	c	3.2	.19	.09	.25	.19	.15	--	39.5	54.8	0.55	31
"	"	"	pc	3.1	.17	.19	.17	.25	.34	--	40.5	55.7	0.91	33
82Fa	Lim	G	pc	3.1	.20	.14	.28	.13	.19	--	41.3	55.5	0.98	30
84Fa^{o}	SAM	G	pc	3.4	.11	.16	.26	.11	.22	.12	40.8	54.8	1.29	57
94Fd^{o}	"	G	pc	2.8	.30	.13	.25	.11	.15	--	41.6	55.1	0.94	17
74Fa^{+}	"	A	pc	3.3	.17	.14	.22	.15	.21	--	40.7	54.7	0.97	35
78R3I^{+}	"	A	pc	2.9	.13	.13	.18	.19	.30	--	41.6	54.1	1.09	41
78R3C	"	A	c	2.8	.04	.11	.24	.16	.18	--	42.0	55.8	0.72	129
"	"	"	pc	2.8	.33	.11	.19	.20	.28	--	42.1	54.8	0.96	15
80Fa	"	G	pc	2.6	.25	.15	.24	.12	.23	--	41.1	54.5	1.35	19
259Fc	SpAM	A	pc	2.7	.48	.14	.17	.21	.27	--	41.4	54.4	0.86	11
263Fa	"	LG	pc	3.0	.29	.14	.15	.20	.21	.08	40.2	55.1	0.74	19

\# A, anorthosite; FD, ferrodiorite; G, gabbro; gg, granophyre; LG, leucogabbro; MG, melagabbro.
* p, primocryst; c, cumulus; pc, postcumulus (average of both early- and late- postcumulus types).
** Atomic ratio.
o Sulfide-bearing.
\+ In anorthosite of reverse cyclic units.

TABLE 9. CHARACTERISTIC ELECTRON-MICROPROBE DATA BY APATITE TYPE (WT%)

Sample no.	Unit or member	F c*	F epc	F lpc	Cl c	Cl epc	Cl lpc	FeO c	FeO epc	FeO lpc	Ce/Y c	Ce/Y epc	Ce/Y lpc
164Fa	LG	3.4			0.02			0.19			1.04		
78B19B	SG	2.9			.13			.29			0.49		
78B19Q	"	3.1			.09			.34			0.42		
78B19U	"	3.3			.10			.33			--		
69Fa	"	3.4			.09			.36			0.42		
70Fa$^{\#}$	Uim		3.1	3.1		0.22	0.20		0.40	0.39		1.33	1.19
71Fb	SG		3.5	3.2		.16	.17		.40	.29		0.92	0.98
72Fa	"		3.1	3.1		.20	.15		.29	.33		1.05	0.91
191Fb$^{\#}$	"		2.5	2.5		.43	.27		.28	.21		1.05	0.91
190Fd	"	3.2		3.0	.16		.21	.19		.16	0.88		0.84
188Fa	"	3.2	3.1		.19	.17		.25	.17		0.55	0.91	
82Fa	Lim		3.0	3.2		.29	.12		.26	.29		1.06	0.89
84Fa$^{\#}$	SAM		3.2	3.5		.12	.10		.28	.23		1.33	1.26
94Fd$^{\#}$	"		2.7	2.9		.32	.28		.23	.27		0.96	0.92
74Fa	"		3.1	3.5		.15	.18		.20	.24		1.03	0.91
78R3I	"		2.9			.13			.18			1.09	
78R3C	"	2.8		2.8	.04		.33	.24		.19	0.72		0.96
80Fa	"		2.5	2.7		.31	.19		.19	.28		1.32	1.42
259Fc	SpAM		2.5	2.8		.58	.39		.14	.19		0.87	0.86
263Fa	"		2.8	3.2		.32	.25		.19	.11		0.76	0.71

* c, cumulus; epc, early postcumulus; lpc, late postcumulus.
\# Sulfide-bearing.

sideration of the other elements reported in Table 6. Elements in distinctly lower concentration in the postcumulus apatite are Al, Ba, Mg, Na, Ni, Sc, Sr, Ti, and Zr; concentrations of Hf, V, and the *REE*s are distinctly higher. Considering the more silicic, postcumulus environment, with attendant crystallization of postcumulus plagioclase and pyroxene, the most puzzling data are those for Ti and V, as well as Hf, Ta and Zr. One might have expected the elements in these two groups to have behaved coherently, but they have not.

Electron-microprobe data for apatite are given in Table 8. Samples are arranged in stratigraphic order from the base upward for ease of viewing chemical changes. Although we recognized overgrowths on some apatite grains, most grains lack optical zoning;

random point analyses and traverses across individual grains indicate little intragranular compositional variability. We calculated OH on the basis of F + Cl + OH = 1 in the structural formula for eight oxygen atoms, and confirmed that the common anion-site abundance is F > OH > Cl. Cl and F contents of Dufek apatite show distinct variations and patterns that have led us to conclude that post-magmatic re-equilibration of F and Cl in apatite is generally not significant. Commonly, postcumulus apatite contains more Cl and less F than cumulus apatite. Cl content in postcumulus apatite decreases irregularly upward from 0.29 and 0.48 wt.% in two samples from the SpAM, to 0.18 and 0.19 wt.% in two samples taken just below the Uim. Cl content is only 0.09 to 0.13 wt.% in cumulus apatite in the SG above the Uim, and is negligible (0.01 to 0.02 wt.%) in primocrystic apatite from the LG. Because of its greater abundance, F shows proportionally less change; F increases upward from 2.6 to 3.1 wt.% in postcumulus apatite of the SpAM and SG, to 3.1 to 3.5 wt.% in cumulus apatite above the Uim and in apatite of the LG. These changes are reflected by the F/Cl atomic ratios (Table 8), which range from 11 to 57 (average 26) in postcumulus apatite, 61 to 70 in cumulus apatite, and 72 to 648 (average 429) in apatite of the LG.

The contrast in F/Cl ratios between types of postcumulus apatite (Table 9) supports the conclusion that two stages of residuum crystallization occurred within the postcumulus assemblage; the two types of apatite typically did not equilibrate. In 11 of 13 cases, early-postcumulus apatite contains more Cl and, in 7 of 13 cases, less F than does late-postcumulus apatite in the same rock (Table 9). Following evidence that Cl content decreases with degree of differentiation (*e.g.*, Huntington 1979), the more Cl-rich composition of this euhedral apatite supports our interpretation that it is an early precipitate in the relatively closed, postcumulus environment. An exception to observed chemical trends occurs for postcumulus apatite from sulfide-bearing gabbros (Table 9), which is relatively rich in Cl and poor in F; only one such sample from the SAM contains relatively F-rich, Cl-poor apatite. Local but significant fluctuations in F/Cl ratio may reflect interaction of postcumulus apatite with hydrothermal fluids. Boudreau *et al.* (1986) ascribed Cl-rich apatite from the Bushveld and Stillwater complexes to equilibration with Cl-rich hydrothermal fluids exsolved during solidification of the cumulus pile.

The upper 220 m of the SAM of the Forrestal Range section consists of four distinctive cycles, each initiated by deposition of plagioclase-rich cumulates (anorthosite) in sharp contact above gabbroic cumulates. In contrast, the transition from anorthositic to gabbroic cumulates within the upper three cycles is gradational. As part of our investigation into the variation of apatite chemistry with stratigraphic position, we analyzed early- and late-postcumulus apatite in a suite of 21 samples from Cycle 3 and two samples from the underlying, upper gabbroic cumulates of Cycle 2. At the sampling locality, Cycle 3 consists of 6 m of anorthositic cumulates and 54 m of overlying gabbroic cumulates; the sampling interval ranged from 1 to 5 m. The results summarized in Table 10 show no significant chemical variation within rock type and no significant difference in the concentrations of Fe, La, and Y for anorthositic *versus* gabbroic cumulates. Distinction between early- and late-postcumulus apatite is marginal in these samples; full ranges and overall averages are presented. For 21 samples in which both types of apatite were analyzed, early-postcumulus apatite contains more Cl and has a higher Ce/Y ratio. Surprisingly, apatite in the gabbroic cumulates of Cycles 2 and 3 contains, on average, more than twice the amount of Cl and correspondingly less F than apatite in the anorthositic cumulates at the base of Cycle 3. Cumulate theory does not readily account for the transitional evolution of anorthositic to gabbroic cumulates. Our Cl and F data support the idea that part of the process was influx or turnover of more primitive magma, regardless of the fact that this appears to be an intracycle transition.

The Fe content of apatite shows two generally increasing trends upward: 1) in postcumulus apatite, from 0.15 and 0.17 wt.% FeO in two samples from

TABLE 10. AVERAGED ELECTRON-MICROPROBE DATA FOR EARLY- AND LATE-POSTCUMULUS APATITE IN CYCLE 3 OF THE STEVENS ANORTHOSITE MEMBER (IN STRATIGRAPHIC SUCCESSION)

	FeO	La_2O_3	Ce_2O_3	Y_2O_3	F	Cl	Ce/Y$^\#$	F/Cl$^\#$
Gabbro section (12)*	0.26** (0.18-0.33)	0.11 (0.06-0.14)	0.22 (0.14-0.30)	0.15 (0.10-0.24)	2.84 (2.30-3.30)	0.32 (0.27-0.37)	1.07 (0.66-1.37)	17 (12-20)
Transition sample (1)	0.20	0.14	0.29	0.23	2.90	0.26	0.87	21
Anorthosite section (8)	0.21 (0.17-0.26)	0.11 (0.09-0.14)	0.24 (0.20-0.32)	0.21 (0.16-0.24)	3.14 (2.80-3.50)	0.15 (0.10-0.20)	0.76 (0.62-0.90)	39 (30-52)
Underlying gabbro section (2)	0.21 (0.19-0.23)	0.10 (0.09-0.10)	0.24 (0.19-0.28)	0.17 (0.09-0.24)	2.70 (2.60-2.80)	0.38 (0.28-0.48)	1.13 (0.80-1.45)	15 (10-19)

$^\#$ Atomic ratio.

* Number of samples.

** Average weight percentage; range given beneath.

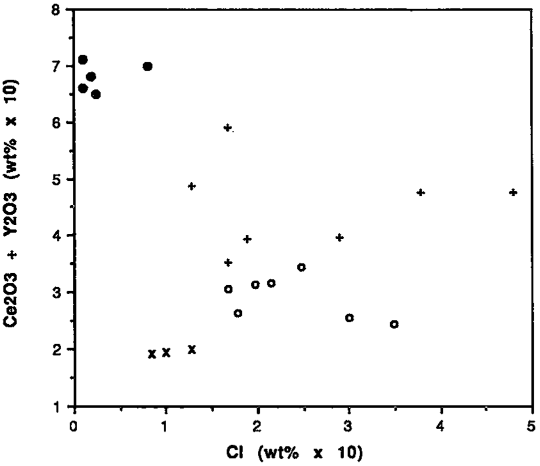

FIG. 8. Plot of Cl against (Ce_2O_3 + Y_2O_3), showing distinction among Dufek apatite occurrences. Symbols: × cumulus apatite, ○ postcumulus apatite in gabbro, + postcumulus apatite in anorthosite, and • primocrystic apatite in the Lexington Granophyre.

the SpAM, to 0.31 and 0.35 wt.% FeO in two samples taken just below the Uim, and 2) in the LG, from 0.16 to 0.45 wt.% FeO. There is no distinction in Fe concentration between postcumulus apatite below the Uim and cumulus apatite above the Uim, or between late-postcumulus apatite and early-postcumulus apatite (Table 9). The lowest Fe contents characterize apatite in anorthosite (Table 8).

Analyses were made for Ce, La, and Y to monitor *REE* abundance and fractionation in apatite. Because preliminary data showed that *REE* abundances are low, we used the greater natural abundance of Y (a Ho homologue) to enable use of Ce/Y atomic ratios as an indicator of *REE* fractionation. *REE* abundances are highest in primocrystic apatite of the LG and lowest in cumulus apatite of the uppermost SG (Table 8, Fig. 8). The *REE*s are more abundant in postcumulus apatite from anorthosite (and leucogabbro) than in that from gabbro (Fig. 8). The Ce/Y atomic ratio is uniformly higher (1.07–1.33) for apatite in the LG and unusually low (0.42) for cumulus apatite in the uppermost SG. For the remaining cumulates, Ce/Y ranges irregularly from 0.74 to 1.37. In 9 of 11 samples (Table 9), the Ce/Y ratio is slightly higher in early-postcumulus apatite than in late-postcumulus apatite.

The large, subhedral abraded apatite grains that we interpret as recycled have been analyzed in samples 78R3C, 188Fa, and 190Fd (Table 8). In sample 78R3C of the SAM, this apatite is notably poorer in Cl and has a lower *REE* content and Ce/Y ratio than coexisting postcumulus apatite, supporting different origins for the two types of apatite. Large abraded apatite in the Transitional zone was analyzed in samples 188Fa and 190Fd, taken some 250 m below the main cumulus-apatite horizon. Although not clearly distinct from coexisting, postcumulus apatite in F and Cl contents, these large grains of apparently cumulus apatite contain more Fe, and less Ce and Y (Tables 8, 9). Their composition contrasts notably with the average of four analyses of cumulus apatite of the main cumulus-apatite horizon: Cl, 0.16 and 0.19 *vs.* 0.10; FeO, 0.19 and 0.25 *vs.* 0.33; Ce_2O_3, 0.15 and 0.19 *vs.* 0.09; and Y_2O_3, 0.15 and 0.19 *vs.* 0.12 wt.%. Abraded apatite of the Transitional zone also is characterized by a notably lower F/Cl ratio than that for apatite in sample 78R3C.

Isotope-dilution data for Rb and Sr in nine apatite separates are compiled in Table 7. Sr abundance increases from as little as 176 ppm in postcumulus apatite from near the base of the Forrestal Range section, to as much as 312 ppm in cumulus apatite from above the Uim. Because Sr is concentrated by a factor of about 2 in plagioclase, relatively early-formed cumulus apatite should contain more Sr than postcumulus apatite that crystallized from interstitial liquid. However, because plagioclase also shows a general increase in Sr content upward in the stratigraphic sequence (Ford *et al.* 1986), little can be made of this argument. Analyses of both plagioclase and apatite strongly indicate repeated influx of Sr-enriched magma into the Dufek chamber. Rb/Sr ratios in apatite fluctuate, but generally decrease with stratigraphic height, in contrast to the reverse trend shown by whole-rock Rb/Sr ratios for Dufek gabbros (Ford *et al.* 1986).

SUMMARY AND DISCUSSION

The record of apatite crystallization in the Dufek intrusion is similar to that in other layered mafic intrusions such as the Skaergaard intrusion (Nash 1976, Brown & Peckett 1977), the Bushveld Complex (Wager & Brown 1968, Von Gruenewaldt 1973), and the Kiglapait intrusion (Huntington 1979), where cumulus apatite appears in upper zones that represent more than 90% solidification. Chemical fractionation trends in Dufek apatite are in many ways comparable to those found in other layered mafic intrusions, but the fractionation of F, Cl, and *REE*s between two types of postcumulus apatite has not been documented.

Below the Uim of the Dufek intrusion, apatite occurs chiefly in trace to minor amounts as a postcumulus phase. Isolated occurrences of cumulus apatite, which occur within and just below the Uim, are interpreted to represent short-lived episodes of apatite precipitation, before the onset of major accumulation of cumulus apatite above the Uim. Partial digestion of fallen blocks in the Uim may have altered the composition of the magma, temporarily moving it away from apatite saturation. Apatite abundances decrease systematically upward in the LG, indicating rapid depletion in P in successive batches of residual liquid.

The physical and chemical characteristics of apatite that occurs in cumulates below the Uim are summarized in Table 11. Based on textural relations and mineral chemistry, small euhedral apatite grains that occur in these cumulates are considered an early-crystallizing postcumulus phase. Frequent occurrence of this euhedral apatite in late-postcumulus quartz and K-feldspar suggests that postcumulus pyroxene and Fe,Ti-oxide minerals, and some postcumulus plagioclase, tended to crystallize before apatite and may have sealed interstitial passages. Further crystallization within the trapped interstitial residuum led to precipitation of anhedral apatite that typically was depleted in Cl and Ce, and modestly enriched in F and Fe. Greater abundance of postcumulus apatite in anorthositic and leucogabbroic cumulates appears to correlate with higher proportions of mesostasis in those rock types.

REE data for apatite are related to the stratigraphy of layered mafic intrusions by Nash (1976; Skaergaard), Brown & Peckett (1977; Skaergaard), Huntington (1979; Kiglapait), Roelandts & Duchesne (1979; Bjerkrem–Sogndal), and Boudreau & McCallum (1989; Stillwater). Reported La, Ce, and Y concentrations are generally lower for the Bjerkrem–Sogndal lopolith and Stillwater Complex (except for the J–M Reef horizon), but comparable for the Kiglapait and Skaergaard intrusions. The data of Nash and Brown & Peckett show no systematic variation of *REE* abundance with stratigraphic position, whereas those for strictly cumulus apatite in the Bjerkrem–Sogndal lopolith reveal a distinct evolution (Fig. 7). Atomic Ce/Y ratios calculated from Nash's data range from 0.48 to 1.06 (average 0.70) and are thus in the lower range measured for Dufek apatite. The data of Nash (1972) for noncumulus apatite in the strongly differentiated alkaline Shonkin Sag laccolith are of interest because the chilled margin of the laccolith contains apatite with Ce and La concentrations comparable to those of postcumulus apatite in the Dufek gabbros, whereas *REE* contents of apatite in the LG approach those of the most differentiated syenites in the Shonkin Sag laccolith.

Comparison of our Cl and F data for apatite with those for apatite in other layered mafic intrusions is not straightforward, in part because the lowermost cumulates are not exposed in the Dufek intrusion. Nash (1976) and Brown & Peckett (1977) reported fluorapatite compositions comparable to ours from rocks of the Chilled Margin, Upper Zone, Sandwich Horizon, and Upper Border Group of the Skaergaard intrusion. They reported a comparable significant drop in Cl content in apatite at the base of UZb, coincident with the first appearance of cumulus apatite. Postcumulus apatite of the Lower and Middle Zones of the Layered Series may contain significantly more Cl than we have measured. Cl and F contents of cumulus apatite from the Upper Zone of the Kiglapait intrusion are similar to those we have measured but, again, more Cl-rich apatite is reported from cumulates low in the intrusion (Huntington 1979). Cl and F contents measured by Nash (1972) for apatite in the Shonkin Sag laccolith are similar to those we find in apatite from the mafic rocks of the Dufek intrusion. Although Cl content shows no systematic trend in Shonkin Sag apatite, F content clearly increases in apatite from the more differentiated rocks. Postcumulus apatite from the Stillwater complex is unusually rich in Cl and poor in F, containing over 6 wt.% Cl at levels 2800 m above the base of the intrusion (Boudreau & McCallum 1989). Apatite higher in the Stillwater Complex contains notably less Cl and more F, but the data are so dissimilar to ours as to make comparative statements and arguments extremely speculative.

TABLE 11. CHARACTERISTICS OF APATITE BELOW THE UPPER INCLUSION MEMBER

Early postcumulus (epc) (euhedral)	Late postcumulus (lpc) (anhedral)	Cumulus (subhedral)
Small but well-formed grains (<0.2 mm diameter) that exhibit high L/B ratios (>10 and mostly 15-25). Some partly to wholely engulfed by postcumulus plagioclase overgrowths. Subhedral epc apatite exhibits intergrowth relationships with postcumulus minerals. Typically occurs in clusters in rocks rich in late-postcumulus quartz and K-feldspar. Thus, more common in leucogabbro and anorthosite than in gabbro or melogabbro. May contain infilled cavities. High Cl, Ce, and Y, low FeO and F contents; high Ce/Y.	Fine to coarse granular; fills voids and sometimes intergrown with other postcumulus minerals. Typically wrapped around corners of cumulus minerals. Forms overgrowths on epc apatite. Occurs in all gabbros but less abundant in melagabbros and magnetite cumulates. Low Cl, moderate to high F, high FeO contents; variable but generally intermediate Ce/Y.	Generally larger, with "detrital" appearance including abraded, embayed, fractured, and broken grains. May contain infilled cavities. Stout subhedral shapes, some over 3 mm in length with nearly 1 mm cross sections. May be found in clusters. Low, Cl, Ce, and Y, high FeO and F contents; low Ce/Y.

On the assumption that trace-element concentrations in apatite are controlled by the environment of crystallization, this study emphasizes the importance of careful petrographic observation. Apatite paragenesis must be understood before apatite chemistry is used to evaluate magma evolution, especially in studies of layered cumulates. Consider the relatively uniform and quite distinctive Cl and *REE* composition of cumulus apatite of the uppermost SG, which can be taken to reflect chemistry of the bulk magma at a late stage of crystallization. Aspects of the composition of apatite in this main cumulus-apatite horizon, and its chemical distinction from postcumulus apatite in underlying cumulates, are remarkably comparable in the Dufek, Skaergaard (Brown & Peckett 1977), and Kiglapait (Huntington 1979) intrusions. In each case, Cl content drops below 0.1 wt.% in cumulus apatite from significantly higher values in postcumulus apatite in underlying cumulates. Total *REE* content and *REE*-distribution patterns in abundant cumulus apatite are comparable in the Dufek, Kiglapait, Skaergaard, and Bjerkrem–Sogndal intrusions, and, in the two intrusions for which data are available (Dufek and Skaergaard), notably lower than in postcumulus apatite in underlying cumulates. Such comparable data, and the regular evolution in cumulus apatite chemistry reported for the Bjerkrem–Sogndal lopolith by Roelandts & Duchesne (1979), suggest that cumulus apatite composition may be a valid means of evaluating magma evolution in layered cumulates. Predicted fractionation trends of Fe and *REE* enrichment, and increasing F/Cl and Ce/Y ratios generally are reflected in the apatite data reported here and elsewhere.

In contrast, postcumulus processes take place in a rapidly evolving environment. Within the cumulus pile, the intercumulus liquid may be expected to be enriched in P, Cl, and *REE*s with respect to the bulk magma as crystallization proceeds. Depending on P concentration, apatite may or may not precipitate in this environment. Apatite composition will depend critically on previous crystallization of other postcumulus phases, which will further enhance Cl and *REE* concentrations and may fractionate the *REE*s. If concepts of cumulate theory are correct, convection of interstitial melt may further perturb "normal" fractionation trends. In an ideal intercumulus system, early-postcumulus apatite might be expected to preferentially concentrate Cl, making it more Cl-rich than late-postcumulus apatite. Even in this ideal case, evolution of total *REE* content and *REE* distribution (*e.g.*, Ce/Y ratio) in postcumulus apatite is difficult to predict. Evolution of total *REE* content will be determined by a balance between the tendency of apatite to preferentially extract *REE*s from the intercumulus liquid (Watson & Green 1981) and the rate at which *REE* concentration in that liquid is enhanced by the incompatibility of *REE*s in other crystallizing phases. Similarly, Ce/Y ratio will be controlled by the balance between relative depletion of *LREE*s by early crystallization of apatite and relative depletion of *HREE*s by crystallization of postcumulus pyroxene. Data reported here and elsewhere show much unexplained variability in the chemistry of postcumulus apatite. We suggest that this variability should not be surprising and emphasize that apatite paragenesis, *i.e.*, the timing of apatite crystallization and the phases with which it crystallizes, is critical to intelligent interpretation of apatite data.

ACKNOWLEDGEMENTS

We appreciate the constructive comments of Mary Donato, Glen Himmelberg, Howard Jaffe, Robert Martin, Alexander McBirney, Eric Sonnethal, and an anonymous reviewer.

REFERENCES

ABEL, K.D., HIMMELBERG, G.R. & FORD, A.B. (1979): Petrologic studies of the Dufek intrusion: plagioclase variation. *Antarctic J. U.S.* **14**(5), 5-8.

ALBEE, A.L. & RAY, L. (1970): Correction factors for electron probe microanalysis of silicates, carbonates, phosphates, and sulfates. *Anal. Chem.* **42**, 1408-1414.

ARGIOLAS, R. & BAUMER, A. (1978): Synthèse de chlorapatite par voie hydrothermale: étude de l'influence de la sursaturation sur l'évolution des facies des cristaux. *Can. Mineral.* **16**, 285-290.

BEHRENDT, J.C., DREWRY, D.J., JANKOWSKI, E. & GRIM, M.S. (1981): Aeromagnetic and radio echo ice-sounding measurements over the Dufek intrusion, Antarctica. *J. Geophys. Res.* **86**, 3014-3020.

______, HENDERSON, J.R., MEISTER, L. & RAMBO, W.L. (1974): Geophysical investigations of the Pensacola Mountains and adjacent glacierized areas of Antarctica. *U.S. Geol. Surv., Prof. Pap.* **844**.

BENCE, A.E. & ALBEE, A.L. (1968): Empirical correction factors for the electron microanalysis of silicates and oxides. *J. Geol.* **76**, 382-403.

BOUDREAU, A.E., MATHEZ, E.A. & MCCALLUM, I.S. (1986): Halogen geochemistry of the Stillwater and Bushveld complexes: evidence for transport of the platinum-group elements by Cl-rich fluids. *J. Petrol.* **27**, 967-986.

______ & MCCALLUM, I.S. (1989): Investigations of the Stillwater Complex. V. Apatites as indicators of evolving fluid composition. *Contrib. Mineral Petrol.* **102**, 138-153.

BROWN, G.M. & PECKETT, A. (1977): Fluorapatites from the Skaergaard intrusion, East Greenland. *Mineral. Mag.* **41**, 227-232.

CAMPBELL, I.H. (1987): Distribution of orthocumulate textures in the Jimberlana Intrusion. *J. Geol.* **95**, 35-54.

CAWTHORN, R.G. & WALSH, K.L. (1988): The use of phosphorus contents in yielding estimates of the proportion of trapped liquid in cumulates of the Upper Zone of the Bushveld Complex. *Mineral. Mag.* **52**, 81-89.

DEER, W.A., HOWIE, R.A. & ZUSSMAN, J. (1962): *Rock-forming Minerals.* **3.** *Sheet Silicates.* Longmans, London.

DRAKE, M.J. & WEILL, D.F. (1972): New rare earth element standards for electron microprobe analysis. *Chem. Geol.* **10**, 179-181.

DRINKWATER, J.L., FORD, A.B. & CZAMANSKE, G.K. (1986): Apatites of the Dufek intrusion, a preliminary study. *Antarctic J. U.S.* **20**(5), 66-69.

FORD, A.B. (1970): Development of the layered series and capping granophyre of the Dufek intrusion of Antarctica. *In* Symposium on the Bushveld Igneous Complex and Other Layered Intrusions (D.J.L. Visser & G. Von Gruenewaldt, eds.). *Geol. Soc. S. Afr., Spec. Publ.* **1**, 492-510.

______ (1976): Stratigraphy of the layered gabbroic Dufek intrusion, Antarctica. *U.S. Geol. Surv., Bull.* **1405**-D.

______ & HIMMELBERG, G.R. (in press): Geology and crystallization of the Dufek intrusion. *In* Geology of Antarctica (R.J. Tingey, ed.). Oxford University Press, Oxford, England.

______ & KISTLER, R.W. (1980): K-Ar age, composition, and origin of Mesozoic mafic rocks related to Ferrar Group, Pensacola Mountains, Antarctica. *N.Z. J. Geol. Geophys.* **23**, 371-390.

______, ______ & WHITE, L.D. (1986): Strontium- and oxygen-isotopic study of the Dufek intrusion. *Antarctic J. U.S.* **20**(5), 63-66.

GARDNER, P.M. (1972): Hollow apatites in a layered basic intrusion, Norway. *Geol. Mag.* **109**, 385-391.

GROBLER, N.J. & WHITFIELD, G.G. (1970): The olivine-apatite magnetitites and related rocks in the Villa Nora occurrence of the Bushweld Igneous Complex. *In* Symposium on the Bushveld Igneous Complex and Other Layered Intrusions (D.J.L. Visser & G. Von Gruenewaldt, eds.). *Geol. Soc. S. Afr., Spec. Publ.* **1**, 208-227.

HAENSEL, J.M., JR., HIMMELBERG, G.R. & FORD, A.B. (1986): Plagioclase compositional variations in anorthosites of the lower part of the Dufek intrusion. *Antarctic J. U.S.* **20**(5), 61-63.

HELZ, R.T. (1987): Differentiation behaviour of Kilauea Iki lava lake, Kilauea Volcano, Hawaii: an overview of past and current work. *In* Magmatic Processes: Physicochemical Principles (B.O. Mysen, ed.). *Geochem. Soc., Spec. Publ.* **1**, 241-258.

HENDERSON, P. (1968): The distribution of phosphorus in the early and middle stages of fractionation of some basic layered intrusions. *Geochim. Cosmochim. Acta* **32**, 897-911.

______ (1970): The significance of the mesostasis of basic layered igneous rocks. *J. Petrol.* **11**, 463-473.

HIMMELBERG, G.R. & FORD, A.B. (1976): Pyroxenes of the Dufek intrusion, Antarctica. *J. Petrol.* **17**, 219-243.

______ & ______ (1977): Iron-titanium oxides of the Dufek intrusion, Antarctica. *Am. Mineral.* **62**, 623-633.

HUNTINGTON, H.P. (1979): Kiglapait mineralogy. I. Apatite, biotite, and volatiles. *J. Petrol.* **20**, 625-652.

IRVINE, T.N. (1982): Terminology for layered intrusions. *J. Petrol.* **23**, 127-162.

MCBIRNEY, A.R. (1989) The Skaergaard Layered Series. I. Structure and average compositions. *J. Petrol.* **30**, 363-397.

MORSE, S.A. & ALLISON, J.P. (1986): Correlation between roof and floor cumulates of the Kiglapait intrusion, Labrador. *Geophys. Res. Lett.* **13**, 1466-1469.

NASH, W.P. (1972): Apatite chemistry and phosphorus fugacity in a differentiated igneous intrusion. *Am. Mineral.* **57**, 877-886.

______ (1976): Fluorine, chlorine, and OH-bearing minerals in the Skaergaard intrusion. *Am. J. Sci.* **276**, 546-557.

PARSONS, I. (1987): *Origins of Igneous Layering.* Reidel, Dordrecht, Holland.

PASTER, T.P., SCHAUWECKER, D.S. & HASKIN, L.A. (1974): The behavior of some trace elements during solidification of the Skaergaard layered series. *Geochim. Cosmochim. Acta* **38**, 1549-1577.

REYNOLDS, I.M. (1985): Contrasted mineralogy and textural relationships in the uppermost titaniferous magnetite layers of the Bushveld Complex in the Bierkraal area north of Rustenburg. *Econ. Geol.* **80**, 1027-1048.

ROEDER, P.L. (1985): Electron-microprobe analysis of minerals for rare-earth elements: use of calculated peak-overlap corrections. *Can. Mineral.* **23**, 263-271.

ROELANDTS, I. & DUCHESNE, J.-C. (1979): Rare-earth elements in apatite from layered norites and iron-titanium oxide ore-bodies related to anorthosites (Rogaland, S.W. Norway). *Phys. Chem. Earth* **11**, 199-212.

VON GRUENEWALDT, G. (1973): The Main and Upper Zones of the Bushveld Complex in the Rossenekal area, Eastern Transvaal. *Geol. Soc. S. Afr. Trans.* **76**, 207-227.

WAGER, L.R. (1960): The major element variation of the layered series of the Skaergaard intrusion and a re-estimation of the average composition of the hidden layered series and of the successive residual magmas. *J. Petrol.* **1**, 364-398.

______ (1963): The mechanism of adcumulus growth in the layered series of the Skaergaard intrusion. *Mineral. Soc. Am., Spec. Pap.* **1**, 1-9.

______ & Brown, G.M. (1968): *Layered Igneous Rocks*. Oliver and Boyd, Edinburgh, U.K.

______ & Deer, W.A. (1939): Geochemical investigations in East Greenland. III. The petrology of the Skaergaard intrusion, Kanderdlugssuag, East Greenland. *Medd. om Grønland* **105**(4), 1-352.

Watson, E.B. & Green, T.H. (1981): Apatite/liquid partition coefficients for the rare earth elements and strontium. *Earth Planet. Sci. Lett.* **56**, 405-421.

Wheatley, M.R. & Rock, N.M.S. (1988): SPIDER: A Macintosh program to generate normalized multielement "spidergrams." *Am. Mineral.* **73**, 919-921.

Wyllie, P.J., Cox, K.G. & Biggar, G.M. (1962): The habit of apatite in synthetic systems and igneous rocks. *J. Petrol.* **3**, 238-243.

Received January 8, 1990, revised manuscript accepted June 6, 1990.